scientific reports

OPEN

Multiscale simulation approach to investigate the binder distribution in catalyst layers of high-temperature polymer electrolyte membrane fuel cells

Sung Hyun Kwon[1], So Young Lee[2], Hyoung-Juhn Kim[2], Sung-Dae Yim[3,4], Young-Jun Sohn[3,4] & Seung Geol Lee[1,5✉]

A multiscale approach involving both density functional theory (DFT) and molecular dynamics (MD) simulations was used to deduce an appropriate binder for Pt/C in the catalyst layers of high-temperature polymer electrolyte membrane fuel cells. The DFT calculations showed that the sulfonic acid (SO_3^-) group has higher adsorption energy than the other functional groups of the binders, as indicated by its normalized adsorption area on Pt (-0.1078 eV/Å^2) and carbon (-0.0608 eV/Å^2) surfaces. Consequently, MD simulations were performed with Nafion binders as well as polytetrafluoroethylene (PTFE) binders at binder contents ranging from 14.2 to 25.0 wt% on a Pt/C model with H_3PO_4 at room temperature (298.15 K) and operating temperature (433.15 K). The pair correlation function analysis showed that the intensity of phosphorus atoms in phosphoric acid around Pt ($\rho_P g_{Pt-P}(r)$) increased with increasing temperature because of the greater mobility and miscibility of H_3PO_4 at 433.15 K than at 298.15 K. The coordination numbers (CNs) of Pt–P(H_3PO_4) gradually decreased with increasing ratio of the Nafion binders until the Nafion binder ratio reached 50%, indicating that the adsorption of H_3PO_4 onto the Pt surface decreased because of the high adsorption energy of SO_3^- groups with Pt. However, the CNs of Pt–P(H_3PO_4) gradually increased when the Nafion binder ratio was greater than 50% because excess Nafion binder agglomerated with itself via its SO_3^- groups. Surface coverage analysis showed that the carbon surface coverage by H_3PO_4 decreased as the overall binder content was increased to 20.0 wt% at both 298.15 and 433.15 K. The Pt surface coverage by H_3PO_4 at 433.15 K reached its lowest value when the PTFE and Nafion binders were present in equal ratios and at an overall binder content of 25.0 wt%. At the Pt (lower part) surface covered by H_3PO_4 at 433.15 K, an overall binder content of at least 20.0 wt% and equal proportions of PTFE and Nafion binder are needed to minimize H_3PO_4 contact with the Pt.

Environmentally friendly energy technology needs to be continuously studied to not only solve environmental problems such as climate change but also satisfy increasing energy demand[1]. Among various energy technologies, fuel cells represent an environmentally friendly energy source that can help alleviate environmental problems. Moreover, fuel cells are promising systems for the noise-free supply of steady energy, with fast start-up and with greater power density compared with fossil fuels[2]. In particular, polymer electrolyte membrane fuel cells (PEMFCs) use a polymeric membrane for proton transport in conjunction with the generation of electricity via the conversion of chemical energy stored in fuels such as hydrogen instead of fossil fuels[3–6].

[1]School of Chemical Engineering, Pusan National University, 2, Busandaehak-ro 63beon-gil, Geumjeong-gu, Busan 46241, Republic of Korea. [2]Hydrogen & Fuel Cell Research Center, Korea Institute of Science and Technology, Hwarang-ro 14-gil 5, Seongbuk-gu, Seoul 02792, Republic of Korea. [3]Fuel Cell Laboratory, Korea Institute of Energy Research (KIER), Yuseong-gu, Daejeon 34129, Republic of Korea. [4]Hydrogen Energy Engineering, University of Science and Technology, Yuseong-gu, Daejeon 34113, Republic of Korea. [5]Department of Organic Material Science and Engineering, Pusan National University, 2, Busandaehak-ro 63beon-gil, Geumjeong-gu, Busan 46241, Republic of Korea. ✉email: seunggeol.lee@pusan.ac.kr

PEMFCs are categorized as low-temperature (LT) or high-temperature (HT) PEMFCs depending on their operating temperature[7,8]. LT-PEMFCs have the advantages of higher power densities, quicker start-up, and greater energy conversion efficiencies while generating little noise and operating at temperatures less than 100 °C. However, LT-PEMFCs have disadvantages of poor CO tolerance of the Pt catalyst in their catalyst layers and humidity-dependent performance[9–14]. By contrast, HT-PEMFCs have several advantages related to their higher operating temperature of 100–200 °C. For example, CO poisoning of the Pt catalysts in the catalyst layers of LT-PEMFCs results in substantial degradation of cell performance[15], whereas HT-PEMFCs are more CO-tolerant than LT-PEMFCs because CO molecules do not easily adsorb onto the Pt surface at elevated temperatures[16]. Moreover, humidification in LT-PEMFCs systems is critical to prevent drying of the polymer membrane; by contrast, HT-PEMFCs exhibit less dependence on humidity than LT-PEMFCs because proton transfer in HT-PEMFCs occurs without water dragging[7,16]. Therefore, HT-PEMFCs can be constructed with a simpler system architecture than LT-PEMFCs[7]. However, HT-PEMFCs have disadvantages of lower energy efficiency than LT-PEMFCs because of the slow kinetics of the oxygen reduction reaction (ORR) and the hydrogen oxidation reaction, which can affect cell performance and lower durability by Pt poisoning and increment of Pt particle size[8,17–21]. Therefore, the commercialization of HT-PEMFCs requires improvements in the cell performance and durability of HT-PEMFCs and a reduction of their manufacturing cost.

HT-PEMFCs comprise gas-diffusion layers, catalyst layers, and polymer-based membranes. The polymer-based membranes are usually polybenzimidazole (PBI)-based membranes doped with phosphoric acid (H_3PO_4) to enable proton transport at temperatures greater than the boiling point of water. The catalyst layers consist of a carbon support with a catalyst (typically Pt), a polymer binder, and H_3PO_4. The H_3PO_4 in the catalyst layers not only performs the same role as the H_3PO_4 in the proton-transfer membranes but also participates in electrochemical reactions by adsorbing onto the Pt catalyst. However, carbon corrosion, particle agglomeration, and acid leaching in the catalyst layers of HT-PEMFCs are substantial problems that affect cell performance and durability[20]. The strong adsorption of H_3PO_4 onto the Pt surface can adversely affect cell performance by decreasing the oxygen permeability and interfering with the ORR in the catalyst layers[22]. Moreover, the durability of the Pt and the carbon surface in catalyst layers is strongly affected by H_3PO_4. Notably, Pt particles have been found to be poisoned by phosphate anions in catalyst layers[23], and H_3PO_4 adsorbed onto the Pt surface adversely affects the ORR[24]. Moreover, the durability of the carbon surface is also affected by the distribution of H_3PO_4 in the catalyst layers. The corrosion of the surface of carbon in the cathode was found to be accelerated under prolonged conditions of high temperature, low pH, and high O_2 concentration[25,26]. Therefore, polymer binders have been used to improve the catalyst layers' mechanical properties when integrated into the carbon support and catalyst. Manipulating the polymer binder content of the catalyst layers enables control of the hydrophobicity and hydrophilicity[27]. In particular, increasing the polymer binder content can increase the durability by preventing H_3PO_4 flooding in the catalyst layers[28].

Polytetrafluoroethylene (PTFE)[29–37], polyvinylidene difluoride (PVDF)[29,37], PBI[29,38–41], Nafion[29] and PBI–PVDF blends[29,42,43] have been mainly used as polymer binders to protect catalyst layers, and the content and type of polymer binder can affect cell performance and durability. Jeong et al.[35] reported the optimum PTFE binder with 20 wt% of PTFE binder content for maximizing cell performance of HT-PEMFCs. In addition, Su et al.[29] also reported that ~ 30 wt% of PTFE binder used in HT-PEMFCs. Further investigations of the contents and types of polymer binders are needed to improve cell performance and durability.

Therefore, in the present study, we conducted a molecular dynamics (MD) simulation for the system of catalyst layers in a HT-PEMFC to improve their binding durability. MD simulation methods have been efficiently used to investigate the structures and diffusion properties of H_3PO_4 in HT-PEMFC membranes[44,45]. For example, H_3PO_4-doped meta-PBI and para-PBI membranes in a HT-PEMFC were investigated, which led to the discovery of a hydrogen bond network for proton transport[44]. In another study, the diffusion coefficients of H_3PO_4 and dihydrogen phosphate anion ($H_2PO_4^-$) in poly(2,5-benzimidazole) (ab-PBI) were investigated with various doping levels of H_3PO_4 to elucidate the proton transfer mechanism[45]. Notably, MD simulation methods have been used to investigate the detailed distribution of polymer binders and H_3PO_4 in catalyst layers[46,47]. The results of such MD simulations have indicated that a suitable amount of PTFE binder is required to prevent H_3PO_4 from reaching the Pt–C surface and thereby improve the durability of the catalyst layers[47]. The adsorption of H_3PO_4 onto the Pt surface was found to be substantially increased by an increase in temperature from room temperature (298.15 K) to the operating temperature of HT-PEMFCs (433.15 K). A follow-up study on the selection of polymer binders is needed to minimize carbon corrosion and Pt poisoning at the PEMFC operating temperature.

In the present MD simulation study, we used density functional theory (DFT) calculations to find appropriate binder candidate groups for use in the catalyst layers in HT-PEMFCs. In particular, we analyzed the adsorption energy between the binder candidate groups and the Pt/C surface, which strongly influences durability. Moreover, we discovered that the interactions can affect the distribution morphologies of polymer binders on the Pt/C surface with H_3PO_4 and that Nafion binders can protect the carbon surface and Pt particles by preventing excess adsorption of H_3PO_4. For this purpose, we used both PTFE and Nafion binders on a Pt/C surface to demonstrate the advantages of each binder in the presence of H_3PO_4 at room temperature (298.15 K) and at the HT-PEMFC operating temperature (433.15 K).

Simulation methods and model preparation

To select the appropriate binder candidates for the Pt/C in catalyst layers, we performed DFT calculations to determine the adsorption energy between the binder candidate polymers and the components of the catalyst layers, such as the carbon surface and the Pt particles. In addition, we performed full-atomistic MD simulations to describe the binder deposit manufacturing process[35] of the catalyst-layer components, including the Pt/C, H_3PO_4, H_2O, and hydronium (H_3O^+) ions, with PTFE and Nafion binder contents ranging from 14.2 to 25.0 wt%.

DFT simulation for selection of binder candidates. To calculate the adsorption energy of the Pt and carbon surface with binder candidates such as PTFE, PVDF, Nafion, PBI, and ab-PBI, we calculated the DFT adsorption energy using the Vienna ab initio Simulation Package (VASP)[48,49]. The generalized gradient approximation Perdew–Burke–Ernzerhof (GGA-PBE) exchange–correlation functional[50] was used with projector-augmented-wave (PAW) pseudopotentials[51] for all geometry optimizations. An energy cut-off of 400 eV was applied with convergence criteria for force (2.0×10^{-2} eV/Å) and energy (1.0×10^{-5} eV). Moreover, the dipole interaction[52] along the z-axis direction and the DFT-D3 correction of the Grimme scheme[53] were applied to calculate the adsorption energy between the Pt and carbon surfaces and the binder candidates. The periodic boundary conditions (PBCs) were applied to all directions, and the slab of the Pt and carbon surface was constructed using three atomic layers of a Pt (111) slab and graphite layers with cell sizes of $9.612 \times 11.099 \times 30.000$ Å³ and $8.522 \times 9.840 \times 30.000$ Å³, respectively. The k-points of the Pt (111) slab and the carbon surface were set to a $5 \times 5 \times 1$ and $6 \times 5 \times 1$ Monkhorst–Pack k-point meshes[54] which correspond to the actual spacing of ~ 0.02 Å^{-1} to the x- and y-axis of PBCs, respectively. The adsorption energies ($E_{\text{adsorption}}$) between the Pt, carbon surface, and binder candidates were calculated using Eq. (1):

$$E_{\text{adsorption}} = E_{\text{total}} - E_{\text{slab}} - E_{\text{binder}} \tag{1}$$

where E_{total} represents the total energy of the Pt or carbon surface with the adsorbed binder, E_{slab} represents the total slab energy of the three layers of Pt (111) slab and the graphite layers, and E_{binder} represents the energy of the binder candidates in the PBCs. The adsorption energy of each component of the binder candidates was calculated to predict detailed adsorption mechanisms during binder distribution on the Pt/C surface.

Force fields and MD simulations. The modified DREIDING force field[55] was applied to describe the PTFE, Nafion, H_3PO_4, and the carbon surface. The H_2O and the $H3O^+$ ions were modeled using an F3C force field[56] to construct the binder solvent, and a Pt particle was modeled using an embedded atom method (EAM) force field[57] to describe the catalyst system in a HT-PEMFC. The DREIDING and F3C force fields have been successfully used to describe fuel cell systems[47,58–64]. For the nonbonded interaction between a Pt particle and the Nafion or PTFE binder, we used the nonbonded interaction parameters reported by Brunello et al.[65]; for the nonbonded interaction parameters between a Pt particle and H_3PO_4, we used those reported by Kwon et al.[47] The total potential energies (E_{total}) of the HT-PEMFC systems were calculated using Eq. (2):

$$E_{\text{total}} = E_{\text{vdW}} + E_{Q} + E_{\text{bond}} + E_{\text{angle}} + E_{\text{torsion}} + E_{\text{inversion}} + E_{\text{EAM}} \tag{2}$$

where E_{vdW}, E_{Q}, E_{bond}, E_{angle}, E_{torsion}, $E_{\text{inversion}}$, and E_{EAM} represent the van der Waals, electrostatic, bond-stretching, angle-bending, torsion, inversion, and EAM energies, respectively. The large-scale atomic/molecular massively parallel simulator (LAMMPS) code[66] from S. Plimpton at Sandia National Laboratory was used to carry out the entire MD simulation for HT-PEMFC systems. The electrostatic interactions were calculated using the particle–particle particle–mesh method[67]. The charges of the atoms in PTFE, Nafion, and H_3PO_4 were calculated via Mulliken population analysis[68] by DFT calculation. All DFT calculations for charge analyses were conducted using a double numerical basis set with polarization (DNP) function and the GGA-PBE[50] functional using DMol³ in the Materials Studio software[69]. The velocity Verlet algorithm[70] was used with time steps of 0.5 fs and 1.0 fs for evaporation and equilibration MD simulations for integrating equations of atomic motions, respectively.

Model preparation. To construct the catalyst layers in the HT-PEMFCs, the carbon surface and Pt particles were constructed at full-atomistic scale. The carbon surface was constructed using six graphite layers with 10,752 carbon atoms. In addition, a Pt particle with a diameter of 2.6 nm was constructed using 586 Pt atoms with a truncated octahedral shape with eight (111) planes and six (100) planes because the Pt particles of the commercial TEC10E50E Pt/C (Tanaka Kikinzoku Kogyo, TKK) have a diameter of 2.5 ± 0.4 nm[71]. The weight ratio between the Pt particles and the carbon surface was matched to the commercial Pt/C concentration (45.9 wt% Pt in the TKK catalyst)[35]. The Pt particle was placed on the carbon surface with a PBC of $68.18 \times 68.88 \times 500.00$ Å³, and the length of the z-direction was set to 500.00 Å with a sufficient vacuum region to prevent interactions beyond the PBC. The chains of the PTFE and Nafion binders were prepared to have 100 and 10 degrees of polymerization (DP), respectively, so that their molecular weight per chain was approximately the same. The PTFE and PTFE–Nafion binder chains were determined to have contents ranging from 14.2 to 25.0 wt%. To prepare the PTFE and PTFE–Nafion binder solvent, 6687 water molecules with 10 additional $H3O^+$ ions per Nafion chain were used for a solvent. In the binder deposit manufacturing process of the PTFE binder with solvent, an isopropyl alcohol (IPA)–water mixture is typically used to prepare catalyst layers with a PTFE binder[29,33,35,36,72]. Nafion binders have also been deposited using a similar manufacturing process with an IPA–water mixture to prepare catalyst layers[29]. Because the IPA molecules in the IPA–water mixture evaporate more easily than water molecules because of the IPA–water vapor–liquid equilibrium[73], water molecules eventually remain with the PTFE binders after evaporation of the IPA molecules at a 70:30 (w/w) IPA/water composition[46]. Therefore, we assumed that the water molecules can mainly affect the final dispersion morphology of the PTFE and Nafion binders on the Pt/C surface. Thus, the water molecules were used to construct the PTFE and Nafion solvent to reduce the computational cost. The initial models of PTFE and Nafion solvent with different binder contents were generated by the Monte Carlo method using the Amorphous Cell module in the Materials Studio software[69].

To obtain equilibrium structures, the PTFE and Nafion solvent models were distributed on a Pt/C surface and canonical ensemble (NVT) MD simulations were performed for 10 ns at 298.15 K. Evaporation simulations in which the temperature was gradually increased from 298.15 to 333.15 K over 30 ps were then performed by NVT simulation, along with an NVT simulation at 333.15 K over 7 ns for evaporation of the water molecules to deposit

Pt/C	Number of Pt atoms (47.0 wt% in Pt/C)	586				
	Number of C atoms (53.0 wt% in Pt/C)	10,752				
Binder content (wt%)		14.2	17.3	20.0	22.6	25.0
Number of Nafion chains (DP = 10) (M_w = 9969.83)		2–3	1–3	1–4	1–5	1–6
Number of PTFE chains (DP = 100) (M_w = 10,039.40)		2–1	4–2	5–2	6–2	7–2
Number of H_3O^+ molecules		20–30	10–30	10–40	10–50	10–60
Number of H_3PO_4 molecules		1500				

Table 1. Compositions of the Pt/C and H_3PO_4 with PTFE–Nafion binder in the model systems.
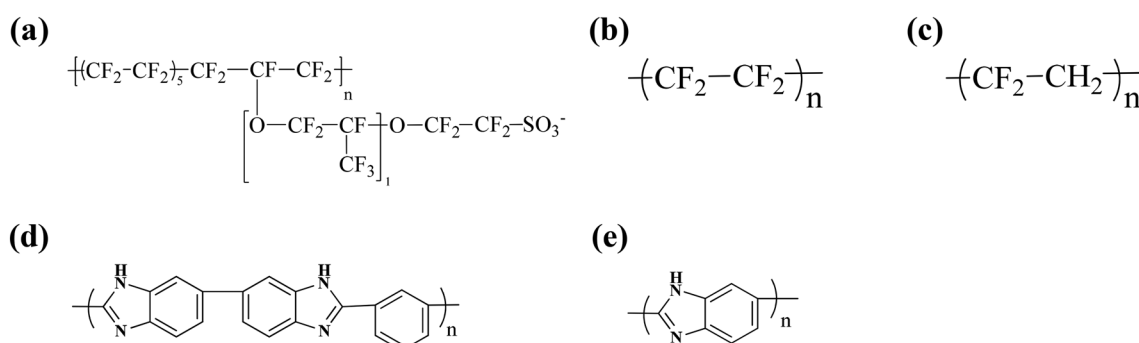
Figure 1. The molecular structures of (**a**) Nafion, (**b**) PTFE, (**c**) PVDF, (**d**) PBI, and (**e**) ab-PBI.

the chains of PTFE and Nafion binder onto Pt/C surface. The temperature was gradually decreased from 333.15 to 298.15 K over 30 ps and 1 ns of NVT simulation at 298.15 K to complete the evaporation simulations. After the evaporation simulations, 1500 molecules of H_3PO_4 were deposited onto a binder–Pt/C surface to construct initial models with H_3PO_4, binder, and a Pt/C surface, where the binder contents ranged from 14.2 to 25.0 wt%. After deposition of the H_3PO_4 molecules, 15 ns of NVT simulations were performed on equilibrated structures at 298.15 and 433.15 K to analyze the detailed changes in the distribution morphologies of H_3PO_4, binder, and the Pt/C surface resulting from a change in temperature. After each equilibration, an additional 5 ns of NVT simulations was performed for data collection. For statistical treatment purposes, at least three independent models were simulated for each case. The detailed molecular composition in our simulations of H_3O^+, PTFE binder, Nafion binder, H_3PO_4, and Pt/C is summarized in Table 1.

Results and discussion
Adsorption properties of binder candidates.
The binder–Pt, binder–carbon surface, H_3PO_4–Pt, and H_3PO_4–carbon surface binding energies strongly affect the distribution of H_3PO_4 on the Pt/C surface[47]. In particular, to prevent excessive contact of H_3PO_4 on the Pt surface and carbon corrosion in the catalyst layers, the binder–Pt and binder–carbon surface adsorption energies should be greater than the H_3PO_4–Pt and H_3PO_4–carbon surface adsorption energies to prevent excess leaching of the carbon surface and Pt particles. We therefore performed DFT calculations to determine and compare the adsorption energies of various binders. Figure 1 shows the molecular structures of the binders, which are commonly used as binders in the catalyst layers of HT-PEMFCs. We prepared the main component in binders for DFT calculations to compare their binding energies on Pt and the carbon surface. In particular, the Nafion (CF_3–O–CF_3, CF_3–SO_3^-, C_4F_{10}), PTFE (C_4F_{10}), PVDF ($C_4H_5F_5$), PBI (benzene, 2,5-benzimidazole), ab-PBI (2,5-benzimidazole) components were calculated on Pt and graphite layers. The results of the binding energies are shown in Table 2. We also normalized the binding energies according to the adsorption areas to enable a quantitative comparison. Figure 2 shows the binding-energy diagram for selecting appropriate binder candidates by comparing the adsorption energy between Pt and the carbon surface on the basis of the adsorption energy of H_3PO_4 (Table 2). The binding energy of H_3PO_4 on the Pt and carbon surfaces is −0.0281 eV/Å^2 and −0.0151 eV/Å^2, respectively. The appropriate binder candidates need to have stronger binding energy than H_3PO_4 on the Pt and carbon surfaces to prevent permeation of H_3PO_4 into the binders. For example, the binding energies between the PTFE binder and the Pt surface (−0.0118 eV/Å^2) and between the PTFE binder and the carbon surface (−0.0085 eV/Å^2) are lower than those between H_3PO_4 and the Pt surface and between H_3PO_4 and the carbon surface. These results mean that the PTFE binder does not readily prevent excessive leaching of the Pt and carbon surfaces in the presence of H_3PO_4 at the HT-PEMFC operating temperature. Therefore, the H_3PO_4 can contact the Pt surface by permeating into the PTFE binder at the HT-PEMFC operating temperature. However, the binding energies between the sulfonic acid groups (SO_3^-) and the Pt surface (−0.1078 eV/Å^2) and between the SO_3^- groups and the carbon surface (−0.0608 eV/Å^2) are much greater than the corresponding H_3PO_4 binding energies. Thus, the SO_3^- groups in Nafion may prevent excess leaching of the Pt and carbon surfaces, thereby improving the mechanical performance and cell durability at the HT-PEMFC operating temperature. We therefore performed MD simulations to investigate the possibil-

4

Materials		Pt(111) surface		Carbon surface	
		Binding energy (eV)	Binding energy (eV/Å²)	Binding energy (eV)	Binding energy (eV/Å²)
Nafion	CF_3-O-CF_3	− 0.362	− 0.0128	− 0.285	− 0.0099
	$CF_3-SO_3^-$	− 2.537	− 0.1078	− 1.409	− 0.0608
Nafion and PTFE	C_4F_{10}	− 0.433	− 0.0118	− 0.313	− 0.0085
PVDF	$C_4H_5F_5$	− 0.635	− 0.0186	− 0.404	− 0.0119
ab-PBI and PBI	ab-PBI	− 2.456	− 0.0571	− 0.640	− 0.0145
	C_6H_6 (benzene)	− 0.937	− 0.0267	− 0.488	− 0.0141
H_3PO_4	H_3PO_4	− 0.618	− 0.0281	− 0.329	− 0.0151

Table 2. The binding energy of components in binders on Pt(111) and carbon surfaces.
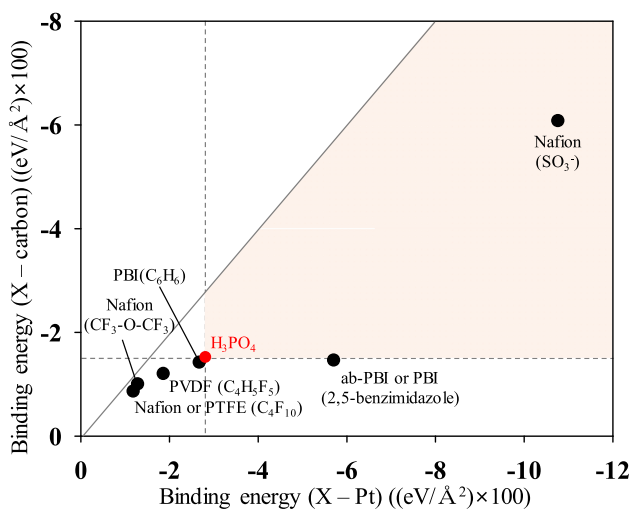
Figure 2. The binding-energy diagram for Nafion, PTFE, PVDF, PBI, and ab-PBI binders.

ity of improving the durability of catalyst layers by controlling the distribution of H_3PO_4 by varying the binder content.

Visualization of evaporated Pt/C structures with binders. Figure 3 shows snapshots of the structures after the evaporation MD simulations. The x- and y-axes indicate the number of PTFE and Nafion chains, respectively, on the Pt/C surface. At the first stage, we conducted the MD simulations with only Nafion binder deposited onto the Pt/C surface to protect both the Pt and the carbon surface by minimizing the adsorption of H_3PO_4. However, the Nafion binder tended to predominantly locate on the Pt surface because of the strong adsorption energy between the Pt and the SO_3^- groups of the Nafion chains. Doo et al.[62] have reported experimental data showing that Nafion strongly adsorbs onto the Pt surface. Thus, Nafion binders can possibly prevent the excess adsorption of H_3PO_4 onto the Pt surface. However, preventing the excess adsorption of H_3PO_4 onto the carbon surface is difficult because of the strong Nafion–Pt interaction. Notably, the authors of another study[47] revealed that a sufficient amount of PTFE binder can prevent the adsorption of H_3PO_4 onto a carbon surface. It means that not only binding energies between PTFE binders and carbon surface, but also distribution procedure is important to form hydrophobicity surface while PTFE binders were preferentially distributed on carbon surface than H_3PO_4. Therefore, not only Nafion but also PTFE binders can be used on Pt/C surfaces to protect both the Pt surface and the carbon surface in the catalyst layers.

As shown in Fig. 3, the influence of the PTFE and Nafion binders was easily identified at low binder contents. For example, simulations for an overall binder content of 14.2 wt% on the Pt/C surface show that more polymer binder with 2 PTFE/2 Nafion chains was attached near the Pt surface than polymer binder with 3 PTFE/1 Nafion chains. By contrast, simulations for an overall binder content of 14.2 wt% also show that more binder with 3 PTFE/1 Nafion chains was attached onto the carbon surface than binder with 2 PTFE/2 Nafion chains. These distribution features show that the PTFE-containing binders positively affect the carbon surface coverage and that the Nafion-containing binders positively affect the Pt surface coverage. With increasing binder content, the Pt and carbon surfaces were gradually covered by PTFE and Nafion binders and each Nafion and PTFE binder was mainly located near the Pt surface and carbon surface, respectively.

We propose a scheme for the distributions of PTFE and Nafion binders on the Pt/C surface. As shown in Fig. 4a, 100% PTFE binder on the Pt/C surface well covers the carbon surface; however, H_3PO_4 still contacted
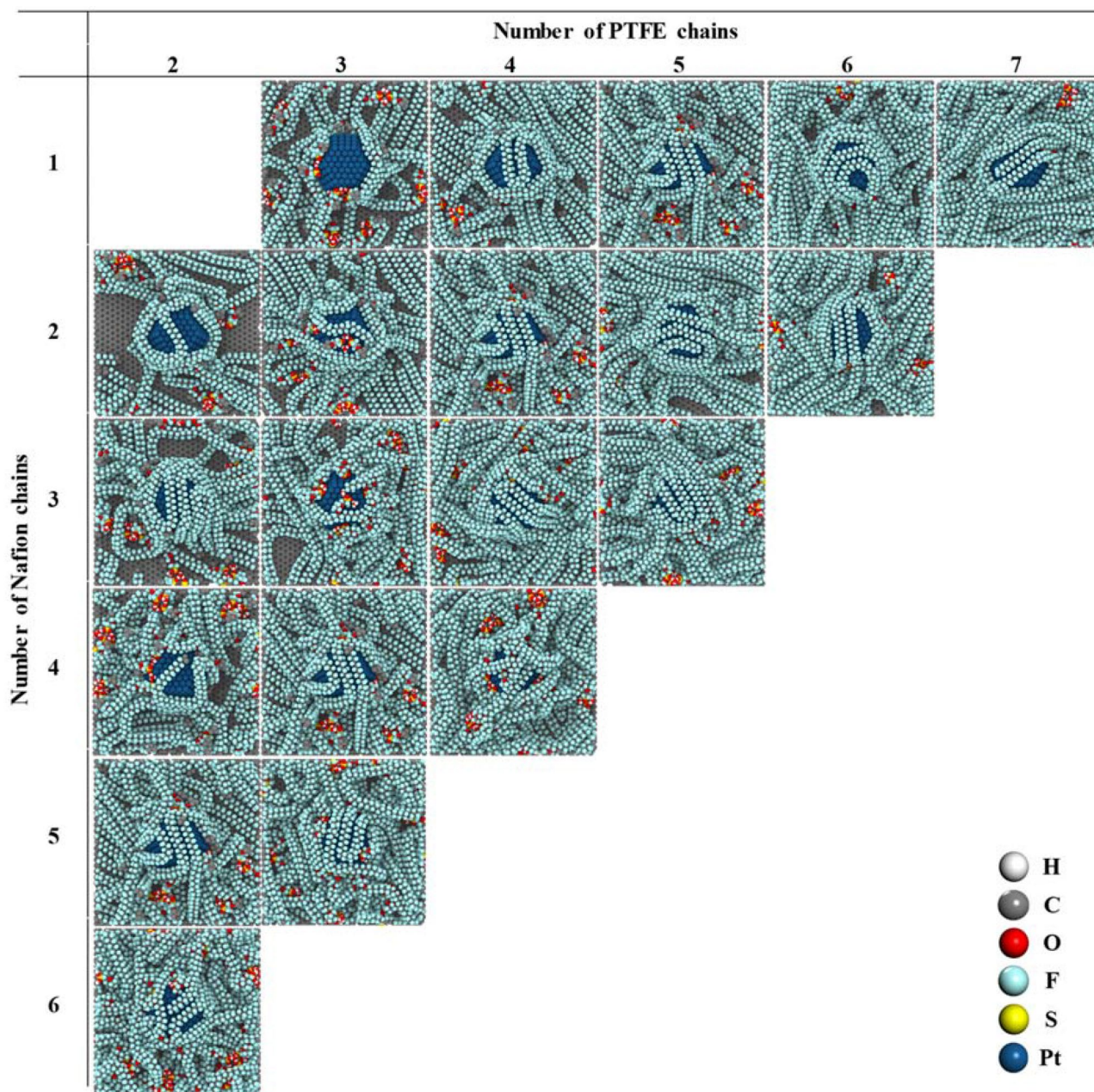
Figure 3. The top view of models after solvent evaporation with various contents (14.2 to 25.0 wt%) of PTFE and Nafion binders on a Pt/C surface. White, gray, red, cyan, yellow, and blue spheres represent hydrogen, carbon, oxygen, fluorine, sulfur, and platinum atoms, respectively.
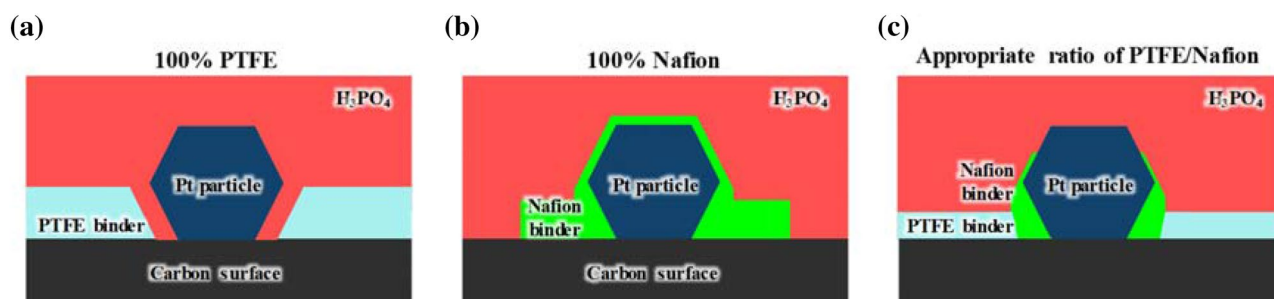

Figure 4. Schematics of binder distribution features for (**a**) 100% PTFE, (**b**) 100% Nafion, and (**c**) an appropriate ratio of PTFE/Nafion binders on the Pt/C surface in a catalyst layer.
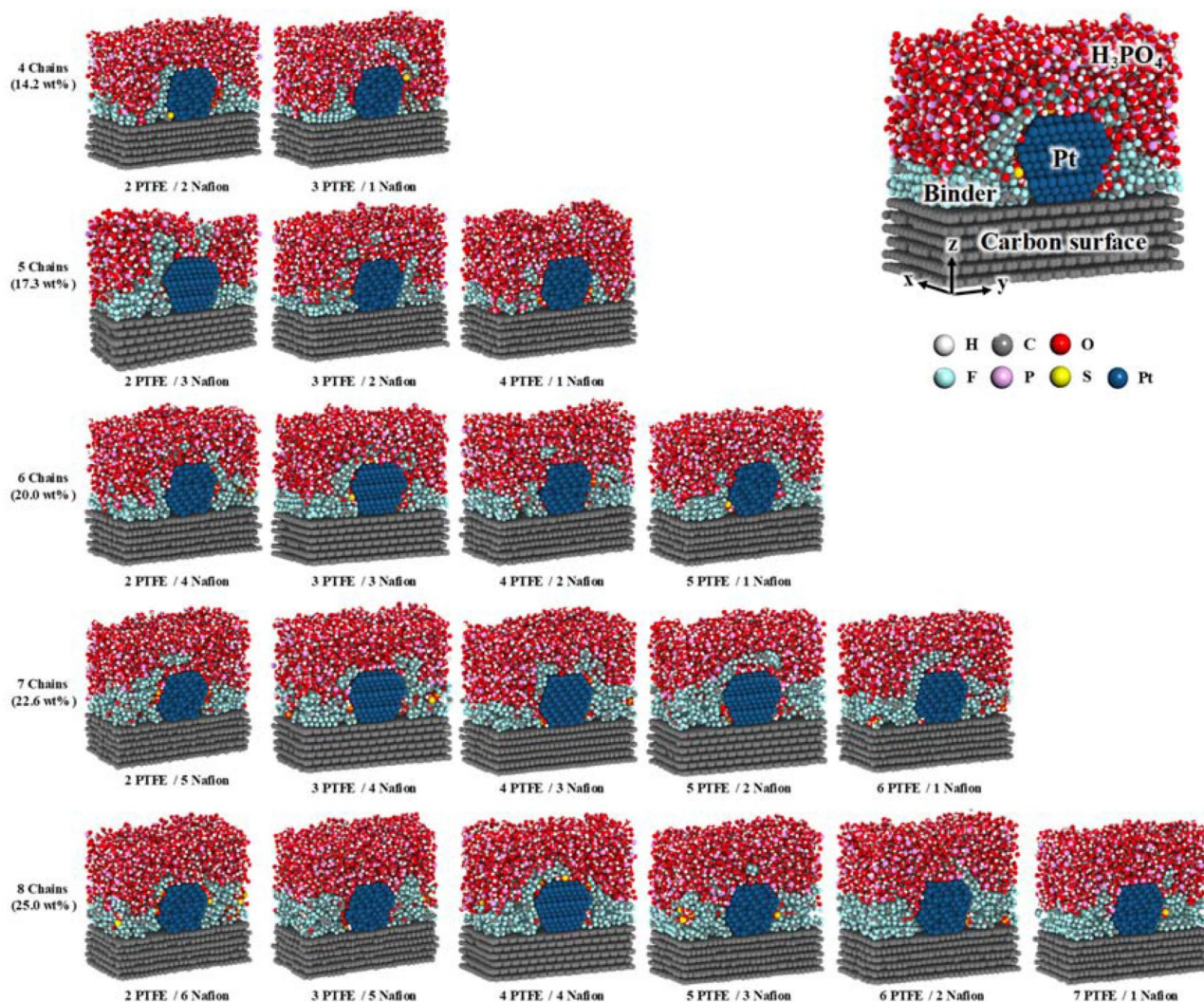
Figure 5. Cross-sectional snapshots of equilibrated Pt/C structures with H_3PO_4 and various contents and ratios of PTFE/Nafion binders at 298.15 K. White, gray, red, cyan, pink, yellow, and blue colors represent hydrogen, carbon, oxygen, fluorine, phosphorus, sulfur, and platinum atoms, respectively.

between carbon and Pt particle surface by pushing out the PTFE binder which located near carbon surface and Pt particles. Thus, although the PTFE binder well protects the carbon surface against carbon corrosion by H_3PO_4, excess PTFE binder is needed to protect the Pt against poisoning by excess adsorption of H_3PO_4 onto the Pt surface. On the contrary, as shown in Fig. 4b, 100% Nafion binder well protects the Pt surface, whereas the Nafion binder poorly protects the carbon because of agglomeration of the SO_3^- groups and strong interaction with the Pt. Therefore, the appropriate PTFE/Nafion binder ratio (Fig. 4c) to protect both the Pt and the carbon surface needs to be determined. Moreover, the total contents of the polymer binders should be reduced to prevent a reduction of the electrical conductivity in the catalyst layers because of the electrical insulating character of the PTFE binder and also to determine the optimum binder content[35]. Therefore, the distribution characteristics of H_3PO_4 as a function of the contents and ratio of PTFE/Nafion binders on the Pt/C surface were evaluated to deduce appropriate structures for improving the durability of HT-PEMFC catalyst layers.

Distribution of H_3PO_4 on Pt/C structures with binders. For catalyst layers consisting of Pt/C and a polymer binder with H_3PO_4, the distribution of H_3PO_4 strongly influences their durability. In particular, excess contact between H_3PO_4 and Pt can cause undesirable effects such as Pt poisoning and carbon corrosion[20,23,25,26]. Therefore, understanding the distributions of H_3PO_4 molecules on the Pt/C surface with PTFE and Nafion–PTFE binders is important for establishing a balance between performance and durability.

Figure 5 shows cross-sectional snapshots of equilibrated Pt/C structures with H_3PO_4 and with PTFE and Nafion binders at contents of 14.2 to 25.0 wt% at 298.15 K. The binders initially covered near the Pt and carbon surface. The binders which are located between Pt and carbon surface can protect the Pt particle and carbon surface by preventing excess adsorption of H_3PO_4 onto the Pt and carbon surfaces. Notably, the distributions of the Nafion and PTFE binders were easily distinguished at low binder contents of 14.2 and 17.3 wt%, where the SO_3^- groups in the Nafion were mainly located near the Pt surface, whereas the PTFE was mainly located near
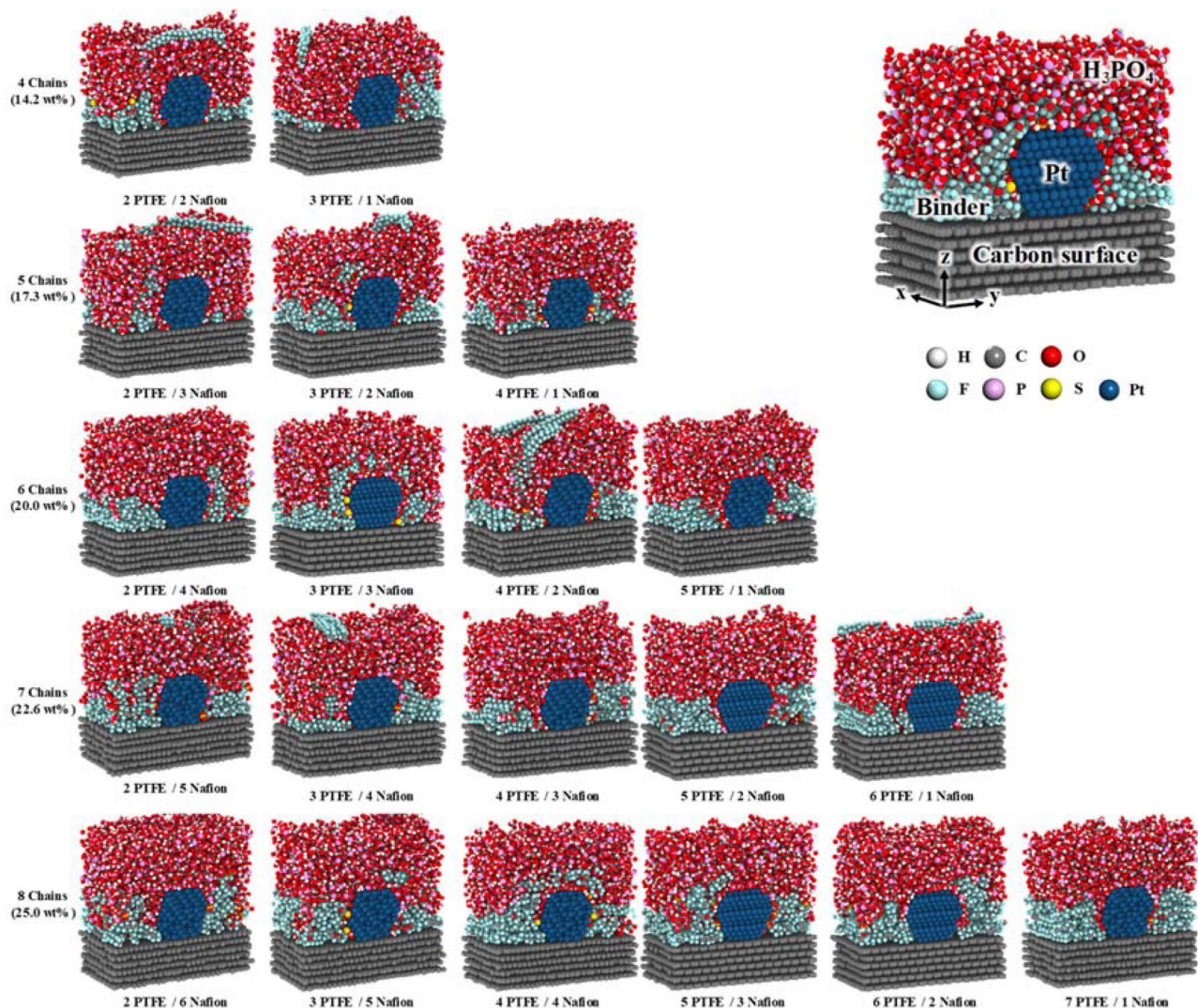
Figure 6. Cross-sectional snapshots of equilibrated Pt/C structures with H_3PO_4 and various contents and ratios of PTFE/Nafion binders at 433.15 K. White, gray, red, cyan, pink, yellow, and blue colors represent hydrogen, carbon, oxygen, fluorine, phosphorus, sulfur, and platinum atoms, respectively.

the carbon surface. For example, at a binder content of 17.3 wt%, the 2 PTFE/3 Nafion binder showed greater contact with the Pt surface than the 4 PTFE/1 Nafion binder. As the binder content was increased, both the PTFE and the Nafion gradually encapsulated the Pt particle and the carbon surface (Fig. 5).

As the temperature was increased from 298.15 K to 433.15 K (HT-PEMFC operating temperature) in Fig. 6, the H_3PO_4 molecules permeated into the binders and contacted the Pt surface. In particular, a high proportion of the PTFE binder was permeated by H_3PO_4 molecules at 433.15 K because H_3PO_4 molecules at this temperatures exhibit greater mobility and miscibility than those at 298.15 K[47] and because the binders located near the Pt and carbon surface was difficult to maintain at this higher temperature. However, the SO_3^- groups in the Nafion binders were still located near the Pt surface even after the increase in temperature because the SO_3^- groups have a higher adsorption energy than H_3PO_4 on the Pt surface.

Structural analysis. The pair correlation functions (PCFs) were evaluated to elucidate the different effects of the PTFE and Nafion binders. The PCF equation is

$$g_{A-B}(r) = \left(\frac{n_B}{4\pi r^2 \Delta r} \right) / \left(\frac{N_B}{V} \right) \tag{3}$$

where $g_{A-B}(r)$ indicates the probability of finding atom A at distance r from atom B in the MD simulations for data collection; n_B is the number of B atoms located at distance r in a shell of thickness Δr from atom A; N_B and V indicate the total number of B atoms in the system and the total volume of the system, respectively; and N_B/V indicates the number density of atom B, ρ_B. The $\rho_B g_{A-B}(r)$ values were used instead of the $g_{A-B}(r)$ values for direct comparisons.
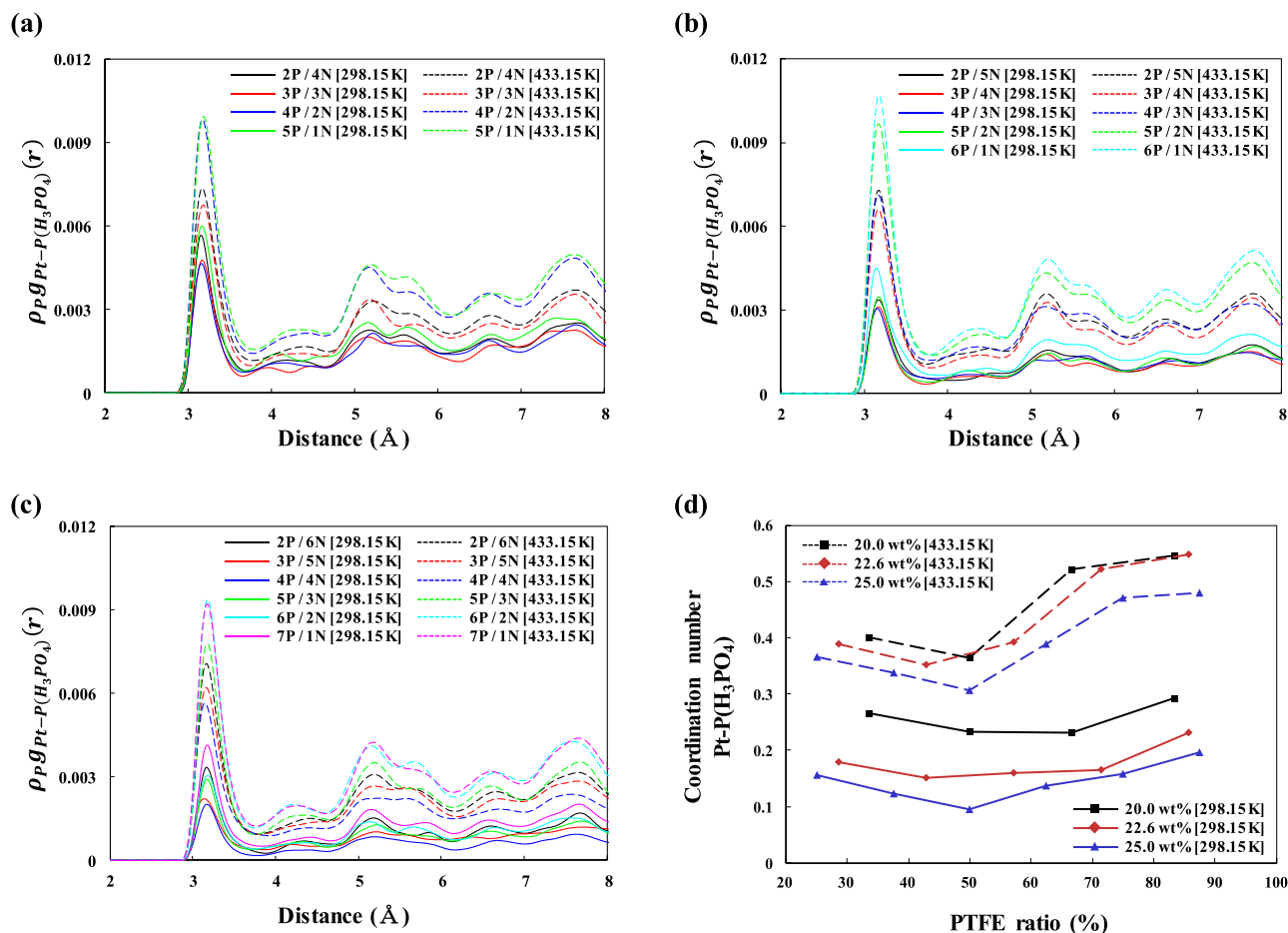
Figure 7. Pair correlation functions ($\rho_P g_{Pt-P}(r)$) of Pt–P(H_3PO_4) at (**a**) 20.0, (**b**) 22.6, and (**c**) 25.0 wt% binder contents with different ratios of PTFE and Nafion binders at 298.15 and 433.15 K. P and N in the legends in (**a**), (**b**), and (**c**) indicate the number of chains of PTFE and Nafion, respectively. (**d**) The coordination numbers (CNs) of Pt–P(H_3PO_4) pairs with different ratios of PTFE and Nafion binders at 298.15 and 433.15 K.

Figure 7a–c shows the PCFs of Pt with H_3PO_4 at binder contents of 20.0, 22.6, and 25.0 wt%, respectively. All intensities of $\rho_P g_{Pt-P}(r)$ increased with increasing temperature from 298.15 to 433.15 K, indicating that the H_3PO_4 molecules were more strongly correlated with the Pt surface at the higher temperature of 433.15 K because the H_3PO_4 molecules exhibit greater mobility and greater miscibility with the PTFE binder[47]. To quantitatively analyze the distribution of H_3PO_4 molecules on the Pt particles as functions of the temperature and the binder ratio, the first coordination numbers (CNs) of Pt–P(H_3PO_4) are shown in Fig. 7d. The CNs were calculated by integrating the first peaks of the intensities of $\rho_P g_{Pt-P}(r)$ in Fig. 7a–c. The intensities of $\rho_P g_{Pt-P}(r)$ decreased as the Nafion ratio was increased to 50% (PTFE 50%). This result means that the adsorption of H_3PO_4 onto the Pt surface decreased with increasing Nafion binder content because of the high adsorption energy between SO_3^- groups and Pt. However, the intensities of $\rho_P g_{Pt-P}(r)$ increased as the Nafion ratio was increased beyond 50% (< PTFE 50%) because the excess Nafion binder agglomerated with itself via its SO_3^- groups. Compared with the CNs of Pt–P(H_3PO_4) at 433.15 K, those at 298.15 K slowly decreased with decreasing PTFE binder ratio (increasing Nafion binder ratio) until the ratio reached 50%. This result means that the Nafion binder more strongly affected the distribution of H_3PO_4 on the Pt surface at 433.15 K than at 298.15 K. Therefore, the distribution of H_3PO_4 molecules in the catalyst layers was apparently more sensitive to the Nafion content than to the PTFE content.

Surface coverage analysis. Not only the distribution of H_3PO_4 on the Pt surface but also its distribution on the carbon surface strongly affects cell durability in HT-PEMFCs because of Pt poisoning and carbon corrosion. Therefore, we also conducted surface analyses to investigate the detailed distribution of H_3PO_4 on the Pt and carbon surfaces as functions of the contents and ratio of PTFE and Nafion binders at 298.15 and 433.15 K. The equation for surface coverage is

$$\text{Surface Coverage (\%)} = (S_{contact}/S_{surface})100 \tag{4}$$

where $S_{contact}$ represents the number of Pt or C atoms in contact with H_3PO_4 molecules and $S_{surface}$ represents the number of Pt or C atoms at the surface of the Pt particle or carbon layer. The contact atoms were counted under the first peak distance of each PCF. Figure 8a,b shows the carbon surface coverage by H_3PO_4 at 298.15 and
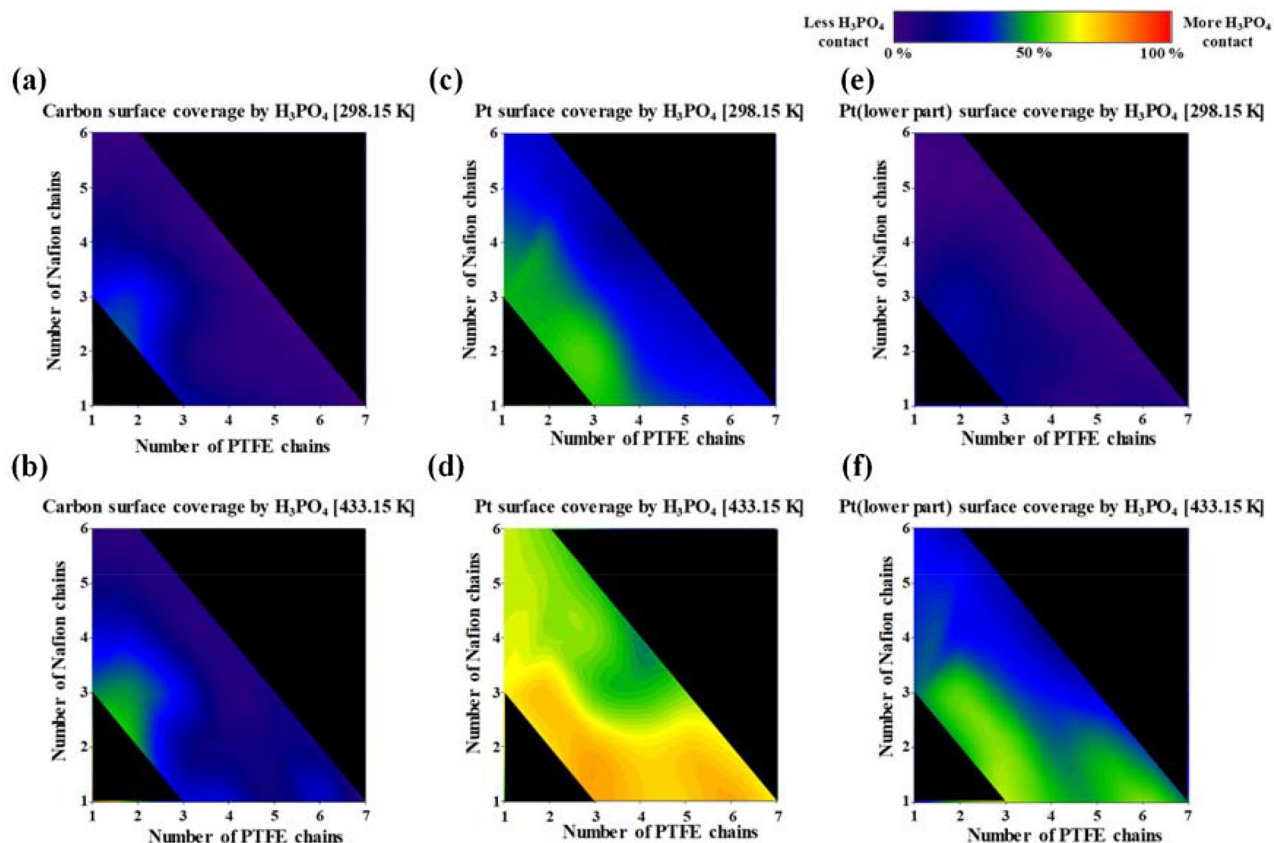
Figure 8. Carbon surface coverage by H_3PO_4 at (**a**) 298.15 K and (**b**) 433.15 K. Pt surface coverage by H_3PO_4 at (**c**) 298.15 K and (**d**) 433.15 K, and the Pt (lower part) surface coverage by H_3PO_4 at (**e**) 298.15 K and (**f**) 433.15 K.

433.15 K, respectively. The distribution of H_3PO_4 molecules on the carbon surface differs depending on the ratio of PTFE and Nafion binders when the binder content is 14.2 wt%. For example, the carbon surface coverage by H_3PO_4 at 14.2 wt% with a high ratio of PTFE (3 PTFE chains and 1 Nafion chain) is lower than that at 14.2 wt% with a high ratio of Nafion (1 PTFE and 3 Nafion chains). These results indicate that the H_3PO_4 molecules were less distributed on the carbon surface with a high ratio of PTFE binders at the same binder content because the PTFE binder was better distributed than the Nafion binder on the carbon surface. Binders with a high ratio of PTFE have the advantage of protecting the carbon surface by preventing the adsorption of H_3PO_4 molecules. By contrast, the Pt surface coverage by H_3PO_4 decreased with increasing Nafion ratio at the same binder content because the Nafion binder tended to locate near the Pt surface because of the strong interactions between the Nafion SO_3^- groups and the Pt. The carbon surface coverage by H_3PO_4 decreased with increasing overall binder content, and no substantial difference was observed in the H_3PO_4 coverage at 298.15 and 433.15 K. Therefore, a binder with at least 20.0 wt% PTFE content should be applied to the Pt/C surface to protect the carbon surface against H_3PO_4 under both 298.15 and 433.15 K temperature conditions. These results were well agreed with experimental data which showed the optimized contents of 20.0–30.0 wt% of PTFE binder[29,35] or ~ 23.0 wt% of Nafion binder[29].

Figure 8c,d shows the Pt surface coverage by H_3PO_4 at 298.15 and 433.15 K, respectively. The Pt surface coverage by H_3PO_4 at 298.15 K decreased with increasing binder content. Notably, at 25.0 wt% binder content, the Pt surface coverage by H_3PO_4 reached the lowest value when the PTFE/Nafion binder ratio was equal (4 PTFE/4 Nafion). This result means that the same ratio of PTFE and Nafion binders with at least 25.0 wt% binder content provided sufficient coverage of both the Pt and the carbon surface to prevent excess adsorption of H_3PO_4. At 433.15 K, binders with a higher ratio of PTFE showed a higher Pt surface coverage by H_3PO_4 than binders with the same ratio of PTFE and Nafion because the PTFE binders were easily permeated by H_3PO_4 as a consequence of the greater mobility of H_3PO_4 and because the adsorption energy of H_3PO_4 on Pt is greater than that of PTFE on Pt. Vice versa, at 433.15 K, binders with a high ratio of Nafion led to lower Pt surface coverage by H_3PO_4 than binders with the same ratio of PTFE and Nafion because the Nafion binder agglomerated with itself via its SO_3^- groups.

We further analyzed the lower Pt surface coverage by H_3PO_4 molecules in Fig. 8e,f because the binders tended to be initially distributed between the lower part of Pt (under half of the Pt layers in Pt particle) and the carbon surface[46]. H_2O molecules near the Pt surface were generated by the reaction of O_2 molecules with protons, and the carbon surfaces in the cathode were corroded in the presence of H_2O under low-pH conditions[26,74] because the H_2O molecules near the lower part of the Pt surface promoted contact between the carbon surface and the

H_3PO_4. At 298.15 K, the lower part of the Pt surface was covered with fewer H_3PO_4 molecules than the upper part of the Pt surface because the binders were mainly distributed between the carbon surface and the Pt[46,47]. At 433.15 K, the binders with a higher ratio of PTFE did not prevent the Pt surface from contacting H_3PO_4 compared with the binders with other ratios because of the lower adsorption energy of PTFE on the Pt surface compared with that of H_3PO_4 on the Pt surface. As the Nafion content in the binders increased at the same overall binder content, the Pt (lower part) surface coverage by H_3PO_4 decreased because of less adsorption of H_3PO_4 onto the lower part of the Pt surface. Therefore, an overall binder content of at least 20.0 wt% with equal PTFE and Nafion contents should be used to protect the lower part of the Pt surface against H_3PO_4 at 433.15 K and thereby improve the durability of the catalyst layers in HT-PEMFCs by protecting the carbon and Pt surfaces.

Conclusions

DFT calculations were performed to determine appropriate binder candidates for protecting Pt/C catalyst layers and thereby improving cell durability. The SO_3^- groups in Nafion appear to make Nafion an appropriate binder candidate because the SO_3^-–Pt and SO_3^-–carbon surface binding energies are greater than the H_3PO_4–Pt and H_3PO_4–carbon surface binging energies. Consequently, we performed full-atomistic MD simulations for binders with various contents (14.2 to 25.0 wt%) of Nafion and PTFE combined in different ratios. The Nafion binders were mainly located near the Pt surface because of higher binding energy of SO_3^- groups with the Pt surface. The intensities of $\rho_{Pg}g_{Pt-P}(r)$ increased with increasing temperature from 298.15 to 433.15 K. At 298.15 K, the coordination numbers of Pt–P(H_3PO_4) decreased more slowly than at 433.15 K with decreasing PTFE binder ratio (increasing Nafion binder ratio) until the ratio reached 50%. The carbon surface coverage by H_3PO_4 almost converged at binder contents greater than 20 wt% at both 298.15 and 433.15 K. The Pt surface coverage by H_3PO_4 was lowest in the case of binders with the same ratio of PTFE and Nafion and at a total binder content 25.0 wt%. For the Pt (lower part) surface coverage by H_3PO_4 at 433.15 K, binders with the same contents of PTFE and Nafion and an overall binder content of at least 20.0 wt% were needed to minimize the H_3PO_4 contact. We expect that our multiscale approach will aid in the selection of other binder candidates for improving the cell durability and the performance of the catalyst layers in HT-PEMFCs.

References

1. Ren, X. F. et al. Current progress of Pt and Pt-based electrocatalysts used for fuel cells. *Sustain. Energy Fuels* **4**, 15–30 (2020).
2. Almeida, T. S., Garbim, C., Silva, R. G. & De Andrade, A. R. Addition of iron oxide to Pt-based catalyst to enhance the catalytic activity of ethanol electrooxidation. *J. Electroanal. Chem.* **796**, 49–56 (2017).
3. Stambouli, A. B. Fuel cells: The expectations for an environmental-friendly and sustainable source of energy. *Renew. Sustain. Energy Rev.* **15**, 4507–4520 (2011).
4. Tanc, B., Arat, H. T., Conker, C., Baltacioglu, E. & Aydin, K. Energy distribution analyses of an additional traction battery on hydrogen fuel cell hybrid electric vehicle. *Int. J. Hydrogen Energy* **45**, 26344–26356 (2020).
5. Li, M. X. et al. Review on the research of hydrogen storage system fast refueling in fuel cell vehicle. *Int. J. Hydrogen Energy.* **44**, 10677–10693 (2019).
6. Tanc, B., Arat, H. T., Baltacioglu, E. & Aydin, K. Overview of the next quarter century vision of hydrogen fuel cell electric vehicles. *Int. J. Hydrogen Energy* **44**, 10120–10128 (2019).
7. Jannelli, E., Minutillo, M. & Perna, A. Analyzing microcogeneration systems based on LT-PEMFC and HT-PEMFC by energy balances. *Appl. Energy* **108**, 82–91 (2013).
8. Pasupathi, S. et al. In *Recent Advances in High-Temperature PEM Fuel Cells* (eds Pasupathi, S/ et al.) 1–5 (Academic Press, 2016).
9. Chen, Q. et al. IS Thermal management of polymer electrolyte membrane fuel cells: A review of cooling methods, material properties, and durability. *Appl. Energy* **286**, 116496 (2021).
10. Wang, Y., Chen, K. S., Mishler, J., Cho, S. C. & Adroher, X. C. A review of polymer electrolyte membrane fuel cells: Technology, applications, and needs on fundamental research. *Appl Energy* **88**, 981–1007 (2011).
11. Peighambardoust, S. J., Rowshanzamir, S. & Amjadi, M. Review of the proton exchange membranes for fuel cell applications. *Int. J. Hydrogen Energy* **35**, 9349–9384 (2010).
12. Steele, B. C. H. & Heinzel, A. Materials for fuel-cell technologies. *Nature* **414**, 345–352 (2001).
13. Kraytsberg, A. & Ein-Eli, Y. Review of advanced materials for proton exchange membrane fuel cells. *Energy Fuel* **28**, 7303–7330 (2014).
14. Wee, J. H. Applications of proton exchange membrane fuel cell systems. *Renew. Sustain. Energy Rev.* **11**, 1720–1738 (2007).
15. Carrette, L. P. L., Friedrich, K. A., Huber, M. & Stimming, U. Improvement of CO tolerance of proton exchange membrane (PEM) fuel cells by a pulsing technique. *Phys. Chem. Chem. Phys.* **3**, 320–324 (2001).
16. Authayanun, S., Mamlouk, M., Scott, K. & Arpornwichanop, A. Comparison of high-temperature and low-temperature polymer electrolyte membrane fuel cell systems with glycerol reforming process for stationary applications. *Appl. Energy* **109**, 192–201 (2013).
17. Liu, Z. Y., Wainright, J. S. & Savinell, R. F. High-temperature polymer electrolytes for PEM fuel cells: Study of the oxygen reduction reaction (ORR) at a Pt-polymer electrolyte interface. *Chem. Eng. Sci.* **59**, 4833–4838 (2004).
18. Li, Q. F., Jensen, J. O., Savinell, R. F. & Bjerrum, N. J. High temperature proton exchange membranes based on polybenzimidazoles for fuel cells. *Prog. Polym. Sci.* **34**, 449–477 (2009).
19. Liu, Z. Y., Wainright, J. S., Litt, M. H. & Savinell, R. F. Study of the oxygen reduction reaction (ORR) at Pt interfaced with phosphoric acid doped polybenzimidazole at elevated temperature and low relative humidity. *Electrochim. Acta* **51**, 3914–3923 (2006).
20. Rosli, R. E. et al. A review of high-temperature proton exchange membrane fuel cell (HT-PEMFC) system. *Int. J. Hydrogen Energy* **42**, 9293–9314 (2017).
21. Qi, Z. G. & Buelte, S. Effect of open circuit voltage on performance and degradation of high temperature PBI-H_3PO_4 fuel cells. *J. Power Sources* **161**, 1126–1132 (2006).
22. Mamlouk, M. & Scott, K. The effect of electrode parameters on performance of a phosphoric acid-doped PBI membrane fuel cell. *Int. J. Hydrogen Energy* **35**, 784–793 (2010).
23. He, Q. G., Shyam, B., Nishijima, M., Ramaker, D. & Mukerjee, S. Mitigating phosphate anion poisoning of cathodic Pt/C catalysts in phosphoric acid fuel cells. *J. Phys. Chem. C* **117**, 4877–4887 (2013).

24. Kaserer, S., Caldwell, K. M., Ramaker, D. E. & Roth, C. Analyzing the influence of H_3PO_4 as catalyst poison in high temperature pem fuel cells using in-operando X-ray absorption spectroscopy. *J. Phys. Chem. C* **117**, 6210–6217 (2013).
25. Dicks, A. L. The role of carbon in fuel cells. *J. Power Sources* **156**, 128–141 (2006).
26. Zhang, S. S. *et al.* A review of accelerated stress tests of MEA durability in PEM fuel cells. *Int. J. Hydrogen Energy* **34**, 388–404 (2009).
27. Zeis, R. Materials and characterization techniques for high-temperature polymer electrolyte membrane fuel cells. *Beilstein J. Nanotech.* **6**, 68–83 (2015).
28. Mazur, P., Soukup, J., Paidar, M. & Bouzek, K. Gas diffusion electrodes for high temperature PEM-type fuel cells: Role of a polymer binder and method of the catalyst layer deposition. *J. Appl. Electrochem.* **41**, 1013–1019 (2011).
29. Su, H. N., Pasupathi, S., Bladergroen, B., Linkov, V. & Pollet, B. G. Optimization of gas diffusion electrode for polybenzimidazole-based high temperature proton exchange membrane fuel cell: Evaluation of polymer binders in catalyst layer. *Int. J. Hydrogen Energy* **38**, 11370–11378 (2013).
30. Mack, F. *et al.* Morphology studies on high-temperature polymer electrolyte membrane fuel cell electrodes. *J. Power Sources* **255**, 431–438 (2014).
31. Wannek, C., Konradi, I., Mergel, J. & Lehnert, W. Redistribution of phosphoric acid in membrane electrode assemblies for high-temperature polymer electrolyte fuel cells. *Int. J. Hydrogen Energy* **34**, 9479–9485 (2009).
32. Wannek, C., Lehnert, W. & Mergel, J. Membrane electrode assemblies for high-temperature polymer electrolyte fuel cells based on poly(2,5-benzimidazole) membranes with phosphoric acid impregnation via the catalyst layers. *J. Power Sources* **192**, 258–266 (2009).
33. Lee, H. J. *et al.* Demonstration of a 20 W class high-temperature polymer electrolyte fuel cell stack with novel fabrication of a membrane electrode assembly. *Int. J. Hydrogen Energy* **36**, 5521–5526 (2011).
34. Mack, F. *et al.* Influence of the polytetrafluoroethylene content on the performance of high-temperature polymer electrolyte membrane fuel cell electrodes. *Int. J. Hydrogen Energy* **41**, 7475–7483 (2016).
35. Jeong, G. *et al.* High-performance membrane-electrode assembly with an optimal polytetrafluoroethylene content for high-temperature polymer electrolyte membrane fuel cells. *J. Power Sources* **323**, 142–146. https://doi.org/10.1016/j.jpowsour.2016.05.042 (2016).
36. Lee, W. J. *et al.* Improvement of fuel cell performances through the enhanced dispersion of the PTFE binder in electrodes for use in high temperature polymer electrolyte membrane fuel cells. *Int. J. Hydrogen Energy* **45**, 32825–32833 (2020).
37. Sasiwimonrit, K. & Chang, W. C. To improve the high temperature polymer electrolyte membrane fuel cells performance by altering the properties of catalyst layer. *Int. J. Hydrogen Energy* **45**, 14491–14499 (2020).
38. Matsumoto, K., Fujigaya, T., Sasaki, K. & Nakashima, N. Bottom-up design of carbon nanotube-based electrocatalysts and their application in high temperature operating polymer electrolyte fuel cells. *J. Mater. Chem.* **21**, 1187–1190 (2011).
39. Lobato, J., Canizares, P., Rodrigo, M. A., Linares, J. J. & Pinar, F. J. Study of the influence of the amount of PBI-H_3PO_4 in the catalytic layer of a high temperature PEMFC. *Int. J. Hydrogen Energy* **35**, 1347–1355 (2010).
40. Seland, F., Berning, T., Borresen, B. & Tunold, R. Improving the performance of high-temperature PEM fuel cells based on PBI electrolyte. *J. Power Sources* **160**, 27–36 (2006).
41. Ong, A. L., Jung, G. B., Wu, C. C. & Yan, W. M. Single-step fabrication of ABPBI-based GDE and study of its MEA characteristics for high-temperature PEM fuel cells. *Int. J. Hydrogen Energy* **35**, 7866–7873 (2010).
42. Zhai, Y. F., Zhang, H. M., Xing, D. M. & Shao, Z. G. The stability of Pt/C catalyst in H_3PO_4/PBI PEMFC during high temperature life test. *J. Power Sources* **164**, 126–133 (2007).
43. Liu, G. *et al.* Studies of performance degradation of a high temperature PEMFC based on H_3PO_4-doped PBI. *J. Power Sources* **162**, 547–552 (2006).
44. Zhu, S. H., Yan, L. M., Zhang, D. F. & Feng, Q. X. Molecular dynamics simulation of microscopic structure and hydrogen bond network of the pristine and phosphoric acid doped polybenzimidazole. *Polymer* **52**, 881–892 (2011).
45. Sun, H., Yu, M. F., Zhao, X. N. & Almheiri, S. Molecular simulation of mass transport in phosphoric acid doped poly(2,5-benzimidazole) polymer electrolyte membranes. *Int. J. Hydrogen Energy* **41**, 7614–7621 (2016).
46. Kwon, S. H., Lee, S. Y., Kim, H.-J., Kim, H.-T. & Lee, S. G. Molecular dynamics simulation to reveal effects of binder content on Pt/C catalyst coverage in a high-temperature polymer electrolyte membrane fuel cell. *ACS Appl. Nano Mater.* **1**, 3251–3258. https://doi.org/10.1021/acsanm.8b00484 (2018).
47. Kwon, S. H., Lee, S. Y., Kim, H.-J., Jang, S. S. & Lee, S. G. Distribution characteristics of phosphoric acid and PTFE binder on Pt/C surfaces in high-temperature polymer electrolyte membrane fuel cells: Molecular dynamics simulation approach. *Int. J. Hydrogen Energy* https://doi.org/10.1016/j.ijhydene.2021.01.218 (2021).
48. Kresse, G. & Furthmuller, J. Efficiency of ab-initio total energy calculations for metals and semiconductors using a plane-wave basis set. *Comp. Mater. Sci.* **6**, 15–50. https://doi.org/10.1016/0927-0256(96)00008-0 (1996).
49. Kresse, G. & Furthmuller, J. Efficient iterative schemes for ab initio total-energy calculations using a plane-wave basis set. *Phys. Rev. B* **54**, 11169–11186. https://doi.org/10.1103/PhysRevB.54.11169 (1996).
50. Perdew, J. P., Burke, K. & Ernzerhof, M. Generalized gradient approximation made simple. *Phys. Rev. Lett.* **77**, 3865–3868 (1996).
51. Payne, M. C., Teter, M. P., Allan, D. C., Arias, T. A. & Joannopoulos, J. D. Iterative minimization techniques for abinitio total-energy calculations—Molecular-dynamics and conjugate gradients. *Rev. Mod. Phys.* **64**, 1045–1097. https://doi.org/10.1103/RevModPhys.64.1045 (1992).
52. Bengtsson, L. Dipole correction for surface supercell calculations. *Phys. Rev. B* **59**, 12301–12304 (1999).
53. Grimme, S., Antony, J., Ehrlich, S. & Krieg, H. A consistent and accurate ab initio parametrization of density functional dispersion correction (DFT-D) for the 94 elements H-Pu. *J. Chem. Phys.* **132**, 154104 (2010).
54. Monkhorst, H. J. & Pack, J. D. Special points for brillouin-zone integrations. *Phys. Rev. B* **13**, 5188–5192 (1976).
55. Mayo, S. L., Olafson, B. D. & Goddard, W. A. DREIDING: A generic force field for molecular simulations. *J. Phys. Chem.* **94**, 8897–8909. https://doi.org/10.1021/j100389a010 (1990).
56. Levitt, M., Hirshberg, M., Sharon, R., Laidig, K. E. & Daggett, V. Calibration and testing of a water model for simulation of the molecular dynamics of proteins and nucleic acids in solution. *J. Phys. Chem. B* **101**, 5051–5061 (1997).
57. Zhou, X. W., Johnson, R. A. & Wadley, H. N. G. Misfit-energy-increasing dislocations in vapor-deposited CoFe/NiFe multilayers. *Phys. Rev. B* **69**, 144113 (2004).
58. Doo, G. *et al.* Tuning the ionomer distribution in the fuel cell catalyst layer with scaling the ionomer aggregate size in dispersion. *ACS Appl. Mater. Interfaces* **10**, 17835–17841 (2018).
59. Lee, J. H. *et al.* Dispersion-solvent control of ionomer aggregation in a polymer electrolyte membrane fuel cell. *Sci. Rep.-Uk* **8**, 10739 (2018).
60. Kwon, S. H. *et al.* Investigating the influence of the side-chain pendants of perfluorosulfonic acid membranes in a PEMFC by molecular dynamics simulations. *Mater. Today Commun.* **21**, 100625 (2019).
61. Kang, H. *et al.* Nanostructures of nafion film at platinum/carbon surface in catalyst layer of PEMFC: Molecular dynamics simulation approach. *J. Phys. Chem. C* **124**, 21386–21395 (2020).
62. Doo, G. *et al.* Nano-scale control of the ionomer distribution by molecular masking of the Pt surface in PEMFCs. *J. Mater. Chem. A* **8**, 13004–13013 (2020).

63. Lee, J. H. *et al.* Controlling ionomer film morphology through altering Pt catalyst surface properties for polymer electrolyte membrane fuel cells. *ACS Appl. Polym. Mater.* **2**, 1807–1818 (2020).
64. Kwon, S. H. *et al.* Effect of perfluorosulfonic acid side chains on oxygen permeation in hydrated ionomers of PEMFCs: Molecular dynamics simulation approach. *Sci. Rep.-Uk* https://doi.org/10.1038/s41598-021-87570-8 (2021).
65. Brunello, G. F. *et al.* Interactions of Pt nanoparticles with molecular components in polymer electrolyte membrane fuel cells: Multi-scale modeling approach. *RSC Adv.* **6**, 69670–69676 (2016).
66. Plimpton, S. Fast parallel algorithms for short-range molecular-dynamics. *J. Comput. Phys.* **117**, 1–19 (1995).
67. Hockney, R. W. & Eastwood, J. W. *Computer Simulation using Particles* (CRC Press, 1988).
68. Mulliken, R. S. Electronic population analysis on LCAO–MO molecular wave functions. I. *J. Chem. Phys.* **23**, 1833–1840. https://doi.org/10.1063/1.1740588 (1955).
69. BIOVIA. *Materials Studio 2019* (Dassault Systèmes, 2019).
70. Swope, W. C., Andersen, H. C., Berens, P. H. & Wilson, K. R. A computer simulation method for the calculation of equilibrium constants for the formation of physical clusters of molecules: Application to small water clusters. *J. Chem. Phys.* **76**, 637–649. https://doi.org/10.1063/1.442716 (1982).
71. Shao, M. H., Peles, A. & Shoemaker, K. Electrocatalysis on platinum nanoparticles: Particle size effect on oxygen reduction reaction activity. *Nano Lett.* **11**, 3714–3719 (2011).
72. Zhang, J. J. *et al.* Enhancing cell performance and durability of high temperature polymer electrolyte membrane fuel cells by inhibiting the formation of cracks in catalyst layers. *J. Electrochem. Soc.* **167**, 114501 (2020).
73. Brunjes, A. S. & Bogart, M. J. P. Vapor-liquid equilibria for commercially important systems of organic solvents: The binary systems ethanol-n-butanol, acetone-water and isopropanol-water. *Ind. Eng. Chem.* **35**, 255–260. https://doi.org/10.1021/ie50398a032 (1943).
74. Pasupathi, S. *et al.* In *Recent Advances in High-Temperature PEM Fuel Cells* (eds Pasupathi, S. *et al.*) 6–18 (Academic Press, 2016).

Acknowledgements

Author contributions

S.H.K. performed the molecular dynamics simulations. S.H.K., S.Y.L. and H.-J.K. analyzed data. S.-D.Y., Y.-J.S. and S.G.L. conceived the research idea. H.-J.K. and S.G.L. designed experiments. S.H.K. and S.G.L. wrote the main manuscript text. S.-D.Y., Y.-J.S. and S.G.L. supervised the research. All authors reviewed the manuscript.

Competing interests

The authors declare no competing interests.

Additional information

Correspondence and requests for materials should be addressed to S.G.L.

Reprints and permissions information is available at www.nature.com/reprints.

Publisher's note Springer Nature remains neutral with regard to jurisdictional claims in published maps and institutional affiliations.